Precipitation projections using a spatiotemporal distributed method: a case study in the Poyang Lake Watershed based on MRI-CGCM3

Ling Zhang [1], Xiaoling Chen[1, 2], Jianzhong Lu[1, *], Dong Liang[1]

[1]State Key Laboratory of Information Engineering in Surveying, Mapping and Remote Sensing, Wuhan University, Wuhan 430079, China

[2]Key Laboratory of Poyang Lake Wetland and Watershed Research, Ministry of Education, Jiangxi Normal University, Nanchang 330022, China

* *Correspondence to*: Jianzhong Lu (lujzhong@whu.edu.cn)

Abstract. Traditional statistical downscaling methods are performed on independent station measurements and ignore spatial correlations and spatiotemporal heterogeneity. In this study, a spatiotemporally distributed downscaling model (STDDM) was developed. Using this method, we interpolated grid observations and GCM (Global Climate Model) simulations to continuously finer grids and then created mapping relationship between the observations and the simulations, respectively for each grid at each time. We applied the STDDM to precipitation downscaling in Poyang Lake Watershed using MRI-CGCM3 (Meteorological Research Institute Coupled Ocean-Atmosphere General Circulation Model3), with an accepted uncertainty of ≤ 4.9%; then created future precipitation changes from 1998 to 2100 (1998-2012 in the historical and 2013-2100 in the RCP8.5 scenario). The precipitation changes increased heterogeneities in temporal and spatial distribution under future climate warming. In terms of temporal patterns, the wet season become wetter while the dry season become drier. The frequency of extreme precipitation increased while that of the moderate precipitation decreased. Total precipitation increased while rain days decreased. The max continuous dry days and the max daily precipitation both increased. In terms of spatial patterns, the dry area exhibited a drier condition during the dry season; the wet area exhibited a wetter condition during the wet season. Analysis with temperature increment showed precipitation changes can be significantly explained by climate warming, with $p < 0.05$ and $R \geq 0.56$. The precipitation changes and explains indicated the downscaling method is reasonable and the STDDM could be applied in the basin-scale region based on a GCM successfully. The results implicated an increasing risk of flood-droughts under global warming, which were a reference for water balance analysis and water resource planting.

1 Introduction

Global warming has caused temporal and spatial redistributions of precipitation (Frei et al. 1998; Trenberth et al. 2011) and has increased the frequency and intensity of floods and droughts, seriously threating social systems and ecosystems (Pall et al, 2000; Dai, 2013). To the fragile ecological and living environments, what the future hydrological situation will be under future global warming is a crucial question to avoid or reduce damages from climate warming.

Global Climate Models (GCMs) are basic tools for assessing the effects of future climate change and provide an initial source for future climates (Xu, 1999). However, GCMs have coarse global resolutions ranging from 1 °×1 ° to 4 °×4 °, and are not applicable in regional scales, such as watersheds. Downscaling algorithms have been developed to link the global-scale GCMs outputs and the regional-scale climate variables, including dynamic (Giorgi, 1990; Teutschbein and Seibert, 2012) and statistic (Wilby et al., 2007; Chu et al., 2010) models. The dynamic method employs regional climate models (RCMs) that are nested inside GCMs based on the complex physics of atmospheric processes and involves high computational costs. Limited by an insufficient understanding of the physical mechanism and expensively computing resources, the dynamic downscaling model cannot easily satisfy small and mid-size region as the Poyang Lake Watershed. Unlike dynamic downscaling, statistic downscaling constructs an empirical relationship between climate variables of the global-scale and local-scale, with inexpensive computations. Benefiting from inexpensive computations and easy implementations, downscaling methods have been widely used, including regression models (Labraga et al. 2010, Quintana et al. 2010; Zorita et al. 1999), weather typing schemes (Bo ǵ et al. 2007; ENKE et al. 2005) and weather generators (Mullan et al., 2016; Baigorria and Jones et al., 2011).

In these studies, statistical downscaling methods have been developed based on the relationship between the global-scale simulations and the local station-scale observations. The methods are conducted on each station, independently. Thus, the specific downscaling relationship and downscaled climate variable are both independent and discrete at the station scale, instead of being spatially continuous at a fine-resolution grid-scale. However, as underlays of local region are complex with different topographies, land covers, and clouds coverage, the downscaling relationships and downscaled climate variables at discrete stations cannot clearly express the spatial heterogeneity, compared to the spatially continuous data. For ungauged areas without station coverage, it is inviable to obtain high-quality downscaling relationships and downscaled local climate

variables. Moreover, the downscaled local climate results and downscaling relationships at the station scale are difficult to show the spatial correlation; however, results from the downscaling, processed on spatially continuous data, such as finer grids, can naturally show spatial relationships. Additionally, spatially continuous data can be directly used in a spatially distributed hydrological model, such as Crest (Wang et al., 2011), VIC (Lohmann et al. 1998), and MIKE SHE (DHI, 2014), which is the forefront of international hydrological scientific research (Beven et al. 1990). In addition, spatially continuous downscaled climate data can be easily integrated with remote sensing data of geologies, topographies, soils, or land covers. In fact, spatially continuous data is widely used in the rapidly developing field of remote sensing, which benefits hydrological models by providing a data source (Engman et al., 1991). Therefore, the downscaling method processed on spatially continuous data is of vital importance. For the continuous space covered with complex underlays, statistical downscaling methods should take spatial heterogeneity into consideration, thus creating downscaling relationships spatially distributed at spatially continuous scale.

In addition to spatial heterogeneity, the relationship between the climate variables at the global-scale and local-scale also shows temporal heterogeneity in a single year, because the dominators that affect climate vary through time (e.g., seasons or months). Therefore, a temporally distributed downscaling method, which creates different relationships at different times, should be taken into consideration. However, many downscaling methods have not taken temporal heterogeneity into consideration. For each observed site, the established downscaling method was a global standard for the whole time, instead of being different in separate seasons or months (Labraga 2010; Wu et al., 2017; Sachindra et al., 2018). In the study, temporally distributed downscaling is considered. Combining temporal heterogeneity and spatial heterogeneity in continual space, a climate downscaling model based on a spatiotemporally distributed framework (a spatiotemporally distributed downscaling method), should be proposed to project future climate at a regional scale.

The Poyang Lake Watershed is sensitive to climate changes in the East Asian monsoon region and therefore is not immune to global warming. Redistributions of precipitation due to global warming have resulted in an increased occurrence of extreme hydrological events, an enhanced flood frequency and intensity (Wang et al., 2009; Guo et al., 2006), a significant decline in lake level and inundation area (Feng et al. 2012; Zhang et al. 2014), which threatened to fragile wetland and forest ecosystems (Han et al. 2015, Dyderski et al. 2018), economic developments and human lives (Ye et al., 2011). However, the Poyang Lake

Wetland ecosystem is an internationally important habitat for migratory birds, abundant of biodiversity and regarded as a Natural Reserve. In addition, the watershed is a commercial grain production area and an important part of the Yangtze River Economic Belt. As this region is economically and ecologically significant, investigating the future precipitation changes in the watershed is crucial for protection from climate damages. Previous studies of future precipitation changes in the Poyang Lake Watershed include temporal and special patterns. Precipitation changes in temporal pattern, focused on intensity and frequency of precipitation extremes (Hong et al. 2014; Wang et al. 2017), as well as the annual or quarterly total precipitation (Guo et al., 2010; Guo et al., 2008; Li et al., 2016). In spatial pattern, precipitation change analysis covers five subbasins (Xinjiang, Raohe, Xiushui, Ganjiang and Fuhe subbasins) (Guo, et al. 2010; Hong, et al. 2014) and 13 discrete meteorological stations (Li et al. 2016), or 7 coarse grids (Guo, et al. 2008). There has been little research concerning the spatial-temporal distribution of precipitation in a continual fine-resolution grids space. In addition, a driving force analysis of precipitation changes related to temperatures increment has not been conducted.

In the study, taking Poyang Lake Watershed as a test case, we projected future precipitations based on the spatiotemporally distributed downscaling method (STDDM), using MRI-GCM3 simulations and meteorological observations. The objects are as the following: (1) to develop a spatiotemporally distributed downscaling method (STDDM), projecting future climate variables in spatially continual scale; and (2) to document temporal and spatial changes in precipitation for the Poyang Lake Watershed in the 21st century and the correlations between these precipitation changes and temperature increment. Future precipitation changes can provide basic hydrological information necessary to a better understanding of water volumes and flood-droughts risks; furtherly benefits wetland and forest ecosystem conservation and aids decision-making in development, utilization, and planning of water resources.

2 Study area and datasets

2.1 Study Area

Poyang Lake Basin (24°28’-30°05’ N and 113°33’-118°29’E) is located in the southeast of China, connected with Yangtze River in the north (Fig. 1). Within the southeast subtropical monsoon zone, the annual average temperature of the watershed

is 17.5℃. The mean annual precipitation is 1638 mm, with 192 rainy days (daily precipitation ≥ 0.1 mm/day) and 173 rain-free days (daily precipitation < 0.1 mm/day). The rainy season lasts from April to July, occupying about 70% of the annual total amount. Inter or intra annual precipitation variations are dominated by the southeast and southwest monsoon, mainly in summer. With a coverage area of 162000 km^2, the diversities of topographies also effect on precipitation changes. The topography varies from high mountains of Luoxiao, Wuyi, and Nanling in east, south and west, with the elevation reaching to the 2200m, to the depressing of Ji Tai or Ganzhou Depressing in the south or center and alluvial plains of Poyang Lake Plain in the north, with the elevation reaching to <50 m (1a). The different topography and location generate the uneven distribution of precipitation in space and produce less rain in the depressing, plains, and hills area because of the leeward sloop, but more orographic rain in the mountain area for the reason of the windward sloop (1b) (Mingjin et al. 2011). To analyze precipitation changes in the rich- or poor-rain area, the meteorological stations were classified into dry and wet stations (Fig. 1a and b), according to the annual precipitation amount. We sorted the annual precipitation averaged over the time from 1961 to 2005, of the 15 stations. The four stations with the max or min mean annual precipitations are set as dry or wet stations, indicating the dry or wet area (Fig.1b), respectively.

In the past 50 years of the Poyang Lake Watershed, annual mean temperature indeed experiences a significant ($p<0.02$) increase with a change rate of 0.15 ℃/10a (Fig.1d), based on the meteorological observations from 1961 to 2005. Under the temperature increasing condition, the precipitation in temporal and spatial distribution becomes more uneven (Zhan et al. 2011), which increases the risk of floods and droughts (Li et al. 2016; Ye et al. 2011).

2.2 Data sets

Global Climate Models (GCMs) are widely used tools to project future climate change. GCMs from the Coupled Model Intercomparison Project Phase Five (CMIP5) performs better than other CMIPs such as CMIP3 and CMIP4, with generally finer resolution and more improved physical mechanism (Sperber, 2013; Taylor et al. 2012). Compared to the other CGMs of CMIP5, the MRI-CGCM3 (Meteorological Research Institute Coupled Ocean-Atmosphere General Circulation Model3, Yukimoto et al. 2012) performs better in simulating diurnal rainfall over subtropical China (Yuan et al. 2013) and has the

finest resolution of 1.121° × 1.125°. Thus we select MRI-CGCM3 data applied in Poyang Lake Watershed to test the performance of the STDDM.

The future data of MRI-CGCM3 includes simulations of the Representative Concentration Pathways (RCPs) of 8.5,6, 4.5 and 2.6. Compared to the other RCPs, in the RCP8.5 scenario temperature increases the most, which is corresponds to a highest greenhouse gas emission, leading to a radiative forcing of 8.5 W/m^2 and temperature increase of 7.14 ℃ at the end of 21st century (Taylor et al. 2012). The research is to detect the remarkable precipitation changes under climate warming; thus we selected future simulations in the RCP8.5 scenario. In the study, we merge the historical (from 1961 to 2005), historical extent (from 2006 to 2012) and RCP85 (from 2013 to 2100) data, as the merged data (1961-2100). To quantitatively analyze the precipitation changes under climate warming in the 21st century, we compared precipitation between the baseline and future period. As annual precipitation observations have main oscillation periods of quasi-20 years (Zhan et al. 2011), we selected three 20 years from the merged data. From the merged data, simulations from 1998 to 2017 were selected as the baseline period data, simulations from 2041 to 2060 were selected as the near future period data, and simulations from 2081 to 2100 were selected as the further future period data.

The local grid observations (Zhao et al., 2014) with a resolution of 0.5 °× 0.5 °are downloaded from the China Meteorological Data Service Center (http://data.cma.cn/). The local grid observations and MRI-CGCM3 historical simulations were used to construct a relationship to correct the GCM data. China metrology point data were also downscaled and used to validate the grid observations and the downscaled GCM simulations. To investigate the relationship between precipitation changes and the temperature increment, we extract not only precipitations but also temperature.

3 Methodology

3.1 Future climate projection based on the spatiotemporally distributed downscaling model

Considering the spatiotemporal heterogeneity of precipitation at the regional scale such as the Poyang Lake Watershed, we developed a spatiotemporally distributed downscaling model (STDDM), which is a logical framework based on a specific mathematic algorithm. The mathematic algorithm was used to create a mapping relationship between the global-scale GCM

simulations and the local scale climates variables. The mapping relationship is used as a transform function to correct the future climate simulations to no-bias data. In the framework, we constructed respective mapping relationships between the match-ups of GCMs simulations and local climate observations in each time (e.g., months or seasons) at each location. The STDDM was improved compared to the traditional downscaling methods by adjusting the specific downscaling algorithm to be suitable in the distributed space and time. Therefore, the downscaling processes show spatiotemporal differences in the parameters or the equations, and the output data are spatially continuous, unlike that in traditional downscaling methods, which ignores the temporal and continuous spatial differences and express space as discrete points instead of continuous grids.

Figure 2a shows the logical framework of the STDDM while Fig. 2b demonstrates how it was applied in Poyang Lake Watershed using MRI-CGCM3 based on a linear-scaling algorithm. The STDDM contains three parts (Fig. 2a and b): (1) upsampling GCMs simulations and local-scale observations to a continuous grid space of the same finer resolution; (2) constructing respective mapping relationship between the GCMs simulations and local observations in distributed space and time; (3) correcting the GCMs simulations using the mapping relationship constructed in step 2.

3.1.1 Upsampling GCMs simulations

MRI-GCM3 simulations were interpolated by Natural Neighbor Interpolation (Sibson et al., 1981) to a scale of 20 km×20 km, the smallest size of the subbasin of the Poyang Lake Watershed (Zhang et al. 2017), generating 263 spatial grids (Fig. 2b). For the spatiotemporally distributed downscaling, we used China meteorology spatially continua grid data as observations, instead of China meteorology station data. We interpolated the gridded observations to 20 km × 20 km, the same as the downscaled climate simulations. The match-up grids of simulations and observations at each time and each grid-box were generated.

3.1.2 Constructing relationships between the GCMs simulations and local observations

Because there is an inevitable mismatch between the simulations and observations (Li, 2009; Wood et al., 2004) after the upsampling, bias correction should be performed. The bias correction was processed by the transform function between match-ups of the upsampled simulation and observations, which represents the mapping relationship between the match-ups. The

transform function could be any bias corrected model, including linear scaling, local intensity scaling, power transformation, distribution mapping models (Teutschbein et al. 2012) and other linear or nonlinear regression models.

As the influencing factors on climates show heterogeneity in space and time, we created spatiotemporally distributed relationships, described by the following formula.

$$C'_{T,S} = F_{T,S}(C_{T,S}) \quad (1)$$

Where, $C'_{T,S}$ and $C_{T,S}$ indicate the upsampled global-scale climate simulations and the local climate variables, respectively, in the given time of *T* and the space of *S*. $F_{T,S}$ demonstrates a transform function, used to correct the upsampled GCMs simulations. The function is a specific bias correction model, spatiotemporally distributed in mathematic equations or parameters, which is constructed based on the data from the historical period of 1961 to 2005.

In this study, we use a linear-scaling algorithm (Lenderink et al., 2007) as the bias correction model. For the linear-scaling algorithm, the simulations were corrected by the discrepancy between the simulations and observations. Precipitations derived from the GCMs were corrected by multiplying the precipitation bias coefficient, which is the ratio of the mean monthly observation to simulation from the historical period; temperatures were corrected by adding the temperature bias coefficient, which is the difference between the mean monthly observation and simulation in the historical period. However, as the bias varies among the months from January to December and among the locations of the 236 spatial grids, a global standard bias coefficient is prohibited. To better capture the bias in distributed time and space, we should create an individual bias coefficient for the given month and gird box. Thus, a spatiotemporally distributed bias matrix was constructed. The respective downscaling model and bias coefficient for a given month (*T*) and space (*S*) were established by Eq. 2 and 3.

$$P' = P \times P\_Cof \quad (2)$$

$$TM' = TM + TM\_Cof \quad (3)$$

where *P* (*T*) represents the precipitation (or temperature) of upsampled simulations. *P'* (*TM'*) represents the downscaled result or upsampled observations; *P_Cof* (*TM_Cof*) represents the bias correction coefficient of precipitations (or temperatures). In the construction of *P_Cof* (*TM_Cof*), *P* (*TM*) and *P'* (*TM'*) was set as the average monthly precipitation (or temperature) over the historical time from 1961 to 2005. All the input and output data in the equations are in the given month (*T*) and space (*S*).

3.1.3 Correcting the GCMs simulations

The constructed relationship between the GCMs simulations and the observations from the historical period (in section 3.1.2) also hold for the future (Maraun et al., 2010). Thus, the transform function was used to correct the future CGCMs simulations. In this study, we corrected the daily and monthly precipitations (or temperatures) from MRI-CGCM3 by adding (or multiplying) the bias coefficients in the corresponding month and grid box.

3.2 Precipitation changes analysis

3.2.1 Statistic indexes of precipitation changes

To obtain the general change in the temporal distribution, we calculated monthly precipitations from 1998 to 2100, averaged over the whole watershed. As floods and droughts occur more frequently in wet and dry months, we specifically analyze the extreme wet and dry precipitation changes in the 21st century. Therein, monthly precipitations, > 75% percentile of the 12 months, were classified as the extreme wet monthly precipitations for each year of the 103 years; monthly precipitations, ≤ 25% percentile were classified as the extreme dry monthly precipitation. The monthly precipitation of the 25%-50% and 50%-75% quantiles were classified as normal dry and wet monthly precipitations. The wet monthly precipitations include extreme and normal wet monthly precipitations; the dry monthly precipitations include extreme and normal dry monthly precipitations. To understand precipitation dynamics in terms of frequency and intensity, daily precipitations were categorized into five classes based on the classification by the Chinese Meteorological Administration and the possible risk of floods and droughts: light rain, medium rain, heavy rain, rainstorm, and extreme rainstorm with daily precipitation of 0.1-10, 10-25, 25-50, 50-100 and >100 mm/day, respectively. The frequency of precipitation intensities indicates heterogeneity in temporal distribution. The higher frequency of moderate rain means the more homogeneous, vice versa is the extreme rain. Therefore, the precipitation intensities were separated to moderate or extreme rains, including light rain, median rain or heavy rain, rainstorm, extreme rainstorm, respectively.

To further analyze the changes in precipitation frequencies and intensities, we calculate the annual days of light rain, medium rain, heavy rain, rainstorm and extreme rainstorm from 1998 to 2100 averaged over the whole watershed. Annual total precipitation, annual dry days, annual max daily precipitation and annual max continuous dry days were displayed as well.

The meteorological stations (Fig. 1a) are uniformly distributed in the whole watershed and cover all kinds of the topographies and land covers. Therefore, in the study, the all above precipitation indexes of one year for the whole watershed were calculated based on the precipitation averaged over the grids containing the 15 stations, instead of the entire grids. Under global climate warming, precipitation becomes more concentrated which leads to more heterogeneity in temporal and spatial distribution (Donat et al., 2016; Min et al., 2011). Thus, we calculated variation coefficients (VC) for each year from 1998 to 2100, to investigate the precipitation changes in temporal and spatial distribution.

The VC is defined as the ratio of the standard deviation to the average value, described by Eq. 4.

$$VC = \frac{\sqrt{\frac{\sum (x-\mu)^2}{n-1}}}{\mu} \tag{4}$$

where x represents monthly (or daily) precipitation in one year; n is the month number (or day number) of a year and μ indicates the average monthly or daily precipitation of a year. VC measures the standard dispersion of the data items, which can indicate the unevenness of temporal and spatial distributions of the precipitation. In this study, heterogeneity in temporal, spatial and spatiotemporal distributions were measured by temporal, spatial and spatiotemporal VC, respectively. Temporal VC was calculated on the daily or monthly precipitations in one year and the VC for one year is averaged over those of the 15 stations. For monthly precipitation, we only select extreme wet and dry precipitations, as the extreme wet and dry are more likely to cause floods or droughts and thus should be paid more attention. Spatial VC was calculated on the annual total precipitations of the 15 stations in one year. Spatiotemporal VC was calculated on the monthly precipitations of the extreme wet months of the wet stations and the extreme dry months of the dry stations in one year, as the extreme precipitation values were more likely to cause floods or droughts.

3.2.2 Relationship analysis between precipitation changes and temperature increasing

We investigated the precipitation changes as a result of global temperature increase. To this end, we made liner regression between the precipitation index and temperature changes from 2005 to 2100. We note that a mean filter with a window size of 21 years can reduce potential random fluctuation from precipitation by the most; thus was used to smooth annual precipitation

indexes and temperature simulations from 2005 to 2100. The long-time smoothed annual precipitation or temperature minus the average annual value from 1998 to 2017, are set as precipitation index or temperature changes. A linear regression model was used to investigate whether precipitation changes are related to climate warming. The two 11 years, 2005 to 2015 and 2090 to 2100 at the start and end, did not have filter diameter of 21 years; thus climate data used to be regressed is from 2016 to 2089.

4 Result and Discussion

4.1 Model assessment

Validation about the China meteorological grid observations should be performed, as well as the STDDM. As the STDDM introduce the China meteorological grid observations and the grid data is not the direct in-suit data, validation about the gridded data is necessary. The determination coefficient (R2), root mean square error (RMSE) and PBias (percent bias) were used to examine the model performance.

4.1.1 Evaluation for the gridded meteorological

The China meteorological grid observations are referenced data to corrected GCMs simulations and reliability of the observations is vital to the performance of the STDDM. So we make a validation using meteorological station observations, in Fig. 3.

As shown in Fig. 3, we select four meteorological stations. The selected stations are uniformly distributed. The validation produced an acceptable precision with $R^2 > 0.91$, absolute PBias < 2% for precipitations and $R^2 = 0.99$, absolute PBias < 6% for temperature. All the dots of gridded and stationed value were distributed along the 1:1 line, thus confirming the satisfactory performance.

4.1.2 Validations of precipitation and temperature projections in Poyang Lake Watershed

Before being used in future climate projection, the model should be examined. Data from 1961 to 1985 were used to construct the model, and the remaining historical data from 1986 to 2005 were used to validate.

To test whether the downscaling method (STDDM) is effective in climate projections, we compare the results before and after the bias correction in Fig. 4. The results before and after the bias correction marked as the outcomes by the STDDM and No-STDDM, respectively. The projections by the STDDM show better performance with high correlations and narrow bias, compared to the result by No-STDDM. Considering the complexity of climate physical mechanism and difficulty to accurately simulate by the present methods, the uncertainty could be acceptable.

Using the STDDM and MRI-CGCMs, we obtained the temporal and spatial variation of future precipitations in the Poyang Lake Watershed, and investigated the heterogeneity changes of precipitation in the temporal and spatial distribution.

4.2 Temporal variation of future precipitation

To discover the temporal variation under the future climate warming, we analyzed the monthly and daily precipitation changes during the period from 1998 to 2100. For monthly precipitation, we analyzed intra-annual and inter-annual dynamics of precipitation; based on the dynamics, we investigated the heterogeneity changes of monthly precipitation. For daily precipitation, we analyzed the changes of precipitation intensities and frequencies; based on the changes, heterogeneity changes of daily precipitation was also investigate.

4.2.1 Monthly precipitation changes

We analyzed the monthly precipitation changes during the period from 1998 to 2100 in Fig. 5. Precipitation show significant intra-annual dynamics. Months with abundant rain (wet months), indicated by a reddish color, are mainly in April to July (the wet season), while the rain-poor months (dry months), indicated by a bluish color, are mainly in September to the subsequent February (the dry season). Precipitation concentrates in spring (March to May) and summer (July to August), occupying 73% of the annual amount. The intra-annual dynamics of precipitation is similar to that shown by Feng (2012). Precipitation also showed inter-annual dynamics. The wet months become wetter, and the wet season comes earlier from April to March, even in February. In addition, each monthly precipitations of seven months (April to November) took increasing trends, of which most months (5 months; April, May, June, August) are in the wet season; while precipitations of the other five months

experienced decreasing trends, all of which were in the dry season. It seems that wet months become wetter and dry months become drier, in general.

To better demonstrate the inter-annual dynamics of precipitation, monthly precipitations in each year were sorted in a descending order in Fig. 5(b). As the time of the monsoon reaching the Poyang Lake Watershed, varied in different years, with 1~2 months' advance or delay; the wet or dry months for different years are not the same. By sorting monthly precipitation, wet months and dry month could be distinguished intuitively in Fig. 5(b). Obviously, monthly precipitation of wet months experienced an increasing trend respectively, even some with slight significance; in contrast, each dry monthly precipitation exhibited decreasing trends, separately, despite the insignificant signs. We accumulated the extreme wet or dry monthly precipitations for each year in Fig. 6. The precipitation of extreme wet months showed a significantly increasing trend ($p<0.05$) (Fig. 6a), while the precipitation of the extreme dry months demonstrated a significantly decreasing trend ($p<0.05$). Extreme wet months increased from 277.82 mm•month^{-1}/a over historical time from 1998-2017, to 344.10 mm•month^{-1}/a over future time from 2081 to 2100, by 23.86% with a change rate of 7.3 mm•month^{-1}/10a. Extreme dry months decreased from 35.44 mm•month^{-1}/a over historical time from 1998-2017, to 30.46 mm•month^{-1}/a over future time from 2081 to 2100, by -14.05% with a change rate of 0.92 mm•month^{-1}/10a. Therein, the extreme wet months are mainly concentrated in March-July (Fig. 6c), part of the wet season, while the extreme dry months are mainly concentrated in September-February (Fig. 6d), consistent to the dry season.

Overall, under climate warming over the 21st century, the wet monthly precipitations become wetter while the dry month precipitations become drier, which suggested the uneven temporal distribution of precipitation (Fig. 7). As shown in Fig. 7, the temporal variation coefficient of the extreme month (including extreme wet and months) precipitations within each year from 1988 to 2100, experiences significantly increasing trends ($p<0.01$), and increased from 0.76 /a over historical time from 1998-2017, to 0.84 /a over future time from 2081 to 2100, by 10.53% with change rate of 0.01 /10a. The significantly increasing trends indicated the more uneven trend of precipitation in the temporal distribution, which might lead to increased risks of floods and droughts.

4.2.2 Daily precipitation changes

To understand the changes in precipitation intensities and frequencies under future climate warming, daily precipitation variations were also analyzed and are shown in Fig. 8. Moderate vs extreme rain frequencies (Fig. 8a and b), the annual total rain vs the annual total rainy days (Fig. 8c), and the annual max precipitation vs the annual max continuous rainy days (Fig. 8d) were analyzed.

Under climate warming, the annual frequency of moderate rains experienced decreasing trends; in contrast, the annual frequency of extreme rains experienced significantly increasing trends (Fig. 8a). Statistically, averaged over 103 years, annual precipitation frequencies are dominated by the moderate rain frequency a total of 163.70 days, or 44.8% (163.70/365), while the extreme rain occurs less often, a total of 20.70 days, or 6.70% (20.7/365). The remaining is rain-free days, a total of 180.75 days, 49.5% (180.75/365). The annual moderate rain frequency decreased, from 170.56 days/a over the historical period from 1998 to 2017, to 159.55 days/a over the future period from 2081 to 2100, by -6.46% with a change rate of -14.4 days/10a; on the contrary, the annual extreme rain frequency increased from 19.18 days/a over historical time from1998 to 2017, to 23.42 days/a over future time from 2081 to 2100, by 22.10% with a change rate of 0.49 days/10a (Fig. 8b).

Furthermore, the annual total rainy days, the sum of the moderate and extreme rain frequencies, demonstrated a significantly decreasing trend in the 21st century, whereas the annual total precipitation exhibited a significantly increasing trend (Fig, 7c). Rainy days decreased from 187.57 days/a over the historical period from 1998 to 2017, to 180.37 days/a over the future period from 2081 to 2100, by -3.84% with a change rate of -1.00 days/10a; while the annual total rain amount increased, from 1650 mm/a over the historical period, from 1998 to 2017, to 1906 mm/a over the future period, from 2081 to 2100, by 15.55% with a change rate of 23.00 mm/10a. The increase in the annual total rain and decrease in the annual rainy days suggested more concentrated precipitation and dry days in the future. This tendency might lead to the increased risk of floods and droughts, which was also indicated by the increased annual max daily precipitation and max continuous dry days (Fig. 8d). Annual max daily precipitation increased from 148.76 $mm \cdot day^{-1}/a$ averaged over the historical period from 1998 to 2017, to 212.01 $mm \cdot day^{-1}/a$ averaged over the future period from 2081 to 2100, by 42.51% with a change rate of 7.2 $mm \cdot day^{-1}/10a$; while the max continuous dry days increased from 25.35 days/a over the historical period from 1998 to 2017, to 28.15 days/a over the future period from 2081 to 2100, by 11.05% with a change rate of 0.5 days/10a.

Overall, the significantly inverse change trends in the moderate vs extreme rain frequencies, the annual total rain vs the annual total rainy days, and the annual max precipitation vs the annual max continuous rainy days, indicated an increasing temporal heterogeneity in precipitation distribution over the 21st century. Obviously, the increasing heterogeneity was exhibited by the increasing temporal VC of daily precipitations (Fig. 9). The temporal VC of daily precipitations increased from 1.50 /a over the historical period from 1998 to 2017, to 1.62 /a over the future period from 2081 to 2100, by 7.48% with a change rate of 0.016 /10a.

4.3 Spatial variation of future precipitation

Climate warming could cause the rain belt shift (Putnam et al., 2017), which might lead to precipitation changes in the spatial pattern. To investigate the spatial variation, we analyzed the similarities and differences of precipitation changes in space (Fig. 1); based on the differences, we use the indexes of the spatial and spatiotemporal VC to investigate the spatial heterogeneity changes (Fig. 11). Fig. 10 shows the precipitation changes in the spatial pattern during the period from 1998 to 2100; Fig. 11 shows the spatial and spatiotemporal VC for each year over 1988 to 2100.

Precipitations showed a regular spatial pattern both in the wet and dry season, in Fig. 10a-c and e-g. More specifically, precipitation was distributed more in the east and west, however less in the north central plain and the south bottom depression. Rich rain in the east and west are dominated by the southeast and southwest summer monsoons. Less precipitation was due to the leeward sloop of the eastern (Xuefeng Mountain) and western mountains (Wuyi Mountain). Less precipitation in the south bottom depression was because that water vapor was blocked from this region by the NanLing Mountain in the south (Fig. 1a). The precipitation distribution in spatial pattern from 1998 to 2100 (Fig. 10 a-c and d-f) were consistent with the observations from 1951 to 2005 (Fig. 1b.), thus confirming the satisfactory performance of the STDDM. Moreover, wet and dry season precipitation showed inverse changes. The wet season precipitations exhibited ascending (Fig. 10a-c and g) change while the dry season precipitation exhibited descending (Fig. 10d-f and h) change from 1998 to 2100. The inverse changes were consistent with the interannual variability of increased precipitation in wet months and decreased precipitation in dry months (Section 4.2). The increase of precipitation in the wet seasons and decrease in precipitation in the dry seasons were also detected in the change rate of the cells over the entire watershed (Fig. 10g or h).

However, precipitation change also showed a different spatial pattern. Precipitation change rate was heterogeneous in spatial distribution for dry or wet season respectively (Fig. 10g and h). In the wet season, the precipitation increased more in the north part of the watershed, except for the central plain (Fig. 10g); in the dry season, the precipitation decreased more in the central area (Fig. 10h). Statistically, in the wet season, precipitation increased with the change rate raising from ≤ 3.6 mm/10a in the southwest, to ≥ 11.7 mm/10a in the northeast; in the dry season, precipitation decreased with the change rate falling from ≥ -2.0 mm/10a in the surrounding region, to ≤ -2.7 mm/10a in the central region. Furthermore, precipitation changes show different spatial characteristics in wet and dry seasons. From 1998 to 2100, in the wet season (Fig. 10a-c), the wet area (the reddish area, mainly in the north except for the center plain) becomes wetter; in the dry season (Fig. 10 d-f), the dry area (the bluish area, mainly in the north center plain and in the south depression) become drier.

The uneven change rates may lead to increase of the spatial heterogeneity of precipitation under global warming, and the tendency of the wet area to become wetter and the dry area to become drier also indicated the increasing spatiotemporal heterogeneity of precipitations. Indeed, the spatial heterogeneity did increase, with the spatial VC raising from 0.097 /a over the historical period (1998-2017), to 0.110 /a over the future period (2081−2100), by 12.64% with a change rate of 0.002 /10a (Fig. 11a). The spatiotemporal heterogeneity did increase with the spatiotemporal VC raising from 0.89 /a over the historical period (1998-2017), to 0.94 /a over the future period (2081-2100), by 4.96% with a change rate of 0.008 /10a. Overall, the uneven change rates for the whole basin and inverse changes for the dry and wet area indicated an increasing spatial heterogeneity in precipitation distribution over the 21st century.

4.4 The impact assessment of temperature increment on precipitation changes

Previous studies have detected precipitation changes and have attributed these changes to climate warming (Westra et al., 2013; Zhang et al., 2013). In this study, the spatiotemporal changes of precipitation in the Poyang Lake Watershed in the 21st century were hypothesized to be related to temperature increments. So we analyze the correlations qualitatively and quantitatively.

The following are trying to demonstrate the driving force related to climate warming on precipitation changes in the temporal pattern. In the wet season from April to July, the summer monsoon might become weaker in Southeast Asia as the temperature increasing (Wang, 2001; Wang, 2002; Guo et al., 2003). Consequently, the summer monsoon is delayed for a longer time in

the middle and lower Yangtze River basin instead of moving further north. The delay leads to much more rain during the wet season. As being located in the middle of the Yangtze River basin, the Poyang Lake Watershed becomes wetter in the wet season (Fig. 5-5, Fig. 10a-c). In fact, the increase in precipitation in the Poyang Lake Watershed was detected in previous studies (Yu and Zhou, 2007; Ding et al., 2008). In the dry period from September to the subsequent February (especially in the winter season, from December to February), during which summer monsoon is inactive, there is less water vapor in the atmosphere to condense into rain. Additionally, stronger winds in the winter (Wu et al., 2013) blow the evaporation away, thus enhancing the difficulty of generating rain from water vapor compared to the other seasons. When temperature increases, the ability of the atmosphere to hold water vapors is strengthened, which makes it more difficult to precipitate. Therefore, precipitation decreases in the dry season, consistent with Li et al.'s (2016) result. As temperature increment increases the ability of the atmosphere to contain water vapor, rain is more difficult, and if it rains it will rain largely (Min et al., 2011; Zhang et al., 2013). Thus, the frequency of heavy rain and rain-free events increases, indicating increased frequency and strengthened intensity of the extreme precipitation. Overall, the climate warming might make precipitation more temporally uneven.

Climate warming could also explain the spatial distribution of precipitation changes in the dry and wet seasons. In the wet season, the summer monsoon delays in the middle and lower Yangtze River Basin. The delaying area covers only the north part of the Poyang Lake Watershed. As it receives abundant water vapor from the delayed summer monsoon, the north part of Poyang Lake Watershed experiences a greater increase in precipitation with a larger change rate (Fig. 10g). The eastern Poyang Lake Watershed is the nearest to the western Pacific Ocean; thus the eastern region receives more continuous water vapor. So the precipitation change rate decreases from the southeast to the northwest in the wet season. However, in the dry season especially in winter, during which there is a low-frequency or absent summer monsoon, the water vapor mainly comes from evapotranspiration. In the watershed, the periphery is covered by the lake of Poyang in the northern plain and high-density vegetation in the northwest, southeast and southwest mountains; so there is more evapotranspiration in the periphery. The center is mainly covered by farmland and grassland; so there is less evapotranspiration in the center (Wu et al., 2013). Thus, the moisture decreases from the surrounding to the center. Therefore, as temperature increases, it is more difficult for rain to occur in the area of lower moisture, the center of the Poyang Lake Watershed. Therefore the precipitation decreased with a change rate falling from the surrounding to the center in the dry season (Fig. 10h).

To quantitatively analyze the relationship between precipitation changes and temperature increment, we created a scatter plot between precipitation indexes changes and temperature increment, as shown in Fig. 12. A trend analysis was conducted using linear regression of each annual precipitation index over the 103 years from 1998 to 2100. The associated slopes represent the change rate of each precipitation index relative to temperature increment. The significance of the trend is indicated by p value. As shown in Fig. 12, there is a significant correlation between the precipitation change and the temperature increment, with $p \leq 0.001$ and $R \geq 0.78$ for 6 precipitation indexes: the annual precipitation in the wet season (Fig. 12a), the annual max daily precipitation (Fig. 12d), the temporal VC of the monthly precipitation (Fig. 12c), the temporal VC of the daily precipitation (Fig. 12f), the spatial VC (Fig. 12g) and the spatiotemporal VC (Fig. 12h). However, changes of the other two precipitation indexes, the annual precipitation in the dry season (Fig. 12b) and the annual max continuous dry days (Fig. 12e), appeared to be correlated with slight signs of $p \leq 0.05$ and $R \leq 0.58$. The overestimation of moderate- or free-rain frequency from the GCM simulations (Teutschbein et al. 2012) might explain the slightly low correlation between the annual precipitation values in the dry season and temperature increment, while the overestimation of the precipitation frequencies (Prudhomme et al. 2003) could explain the slightly low correlation between the annual max continuous dry days and temperature increment. For all the correlations (Fig. 12a-h), the precipitation changed with fluctuation, which might be caused by random variations from GCMs. Overall, despite the low correlations and stochastic fluctuation, the correlations could indicate that the climate warming can partly explain the precipitation changes. Statistically, precipitation changes relative to temperature increment are 16.657 $mm \bullet month^{-1}/K$, -4.31 $mm \bullet month^{-1}/K$, 17.45 $mm \bullet day^{-1}/K$, 0.71 days/K, 0.028/K, 0.033/K, 0.0074/K and 0.02/K for the annual precipitation in the wet season, the annual precipitation in the dry season, the annual max daily precipitation, the annual max continuous dry days, the temporal VC of the monthly precipitation, the temporal VC of the daily precipitation, and the spatial VC and the spatiotemporal VC, respectively.

In summary, the explanation of precipitation changes in temporal and spatial distribution qualitatively and quantitatively, suggests the downscaling method is reasonable and the STDDM could be applied in the basin-scale region based on a GCM successfully.

5 Conclusion

A spatiotemporally distributed downscaling method (STDDM) was proposed in this study. The downscaling method considered the heterogeneity in spatial and temporal distributions, and produced local climate variables as spatially continuous data instead of independent and discrete points. The STDDM showed a better performance than the No-STDDM. Using the STDDM, we constructed the spatially continuous future precipitation distribution and dynamics in the wet and dry season from 1998 to 2100, based on MRI-CGCM3. Several findings were obtained:

First, the spatial and temporal heterogeneity of precipitation increased under future climate warming. In the temporal pattern, the wet season become wetter, while the dry season become drier. The frequency of extreme precipitation increased, while that of the moderate precipitation decreased. Total precipitation increased, while rain days decreased. The max dry day number and the max daily precipitation both increased. These precipitation changes demonstrated an increasing heterogeneity of precipitation in temporal distribution, and the change rate of temporal heterogeneity is 0.01 /10a (0.016 /10a) for the temporal VC of the monthly (daily) precipitation. In the spatial pattern, the change rate of precipitation was uneven over the whole watershed. Additionally, the wet areas become wetter in the wet season and the dry areas become drier in the dry season. The uneven change rates for the whole basin and inverse change for dry and wet area demonstrated an increasing heterogeneity in the spatial distribution, and the change rate of spatial heterogeneity was 0.002/10a.

Second, precipitation changes can be significantly explained by climate warming, with $p < 0.05$ and $R \geqslant 0.56$. The explanation of precipitation changes in temporal and spatial distribution qualitatively and quantitatively, suggests the downscaling method is reasonable and the STDDM could be applied in the basin-scale region based on a GCM successfully.

The results can be applied to a hydrological and hydrodynamic model, to study the future changes in water volumes, lake levels and areas response to climate warming. The relationship between precipitation variations and temperature increment could be helpful to the driving forces analysis of precipitation changes. The dry to be drier and wet to be wetter condition may lead to increased risk of floods and droughts. In particular, in the region where floods and droughts do not usually occur, additional adaptation measures could be taken to prevent loss from the future frequent hydrological disasters.

Data availability

All data can be accessed as described in Sect. 2.2. The data sets and model codes are provided in the supplements.

Acknowledgements

This work was funded by the National Natural Science Funding of China (NSFC) (41331174, 41461080), the National Key Research and Development Program (2017YFB0504103), the Open Foundation of Jiangxi Engineering Research Center of Water Engineering Safety and Resources Efficient Utilization (OF201601), the ESA-MOST Cooperation DRAGON 4 Project (EOWAQYWET), the Fundamental Research Funds for the Central Universities (2042018kf0220) and the LIESMARS Special Research Funding.

Reference

Alexander, L. V., Zhang, X., Peterson, T. ., Caesar, J., Gleason, B., Klein Tank, A. M. G., Haylock, M. R., Collins, W. D. and Trewin, B.: Global observed changes in daily climate extremes of temperature and precipitation, J. Geophys. Res., 111, D05109, doi:10.1029/2005JD006290, 2006.

Baigorria, G. A. and Jones, J. W.: GiST: A Stochastic Model for Generating Spatially and Temporally Correlated Daily Rainfall Data, J. Clim., 23(22), 5990–6008, doi: 10.1175/2010jcli3537.1, 2010.

Beven, K. J.: A Discussion of distributed hydrological modelling, Distrib. Hydrol. Model., 255–278, doi:10.1007/978-94-009-0257-2_13, 1996.

Chen, H. and Sun, J.: How the “best” models project the future precipitation change in China, Adv. Atmos. Sci., 26(4), 773–782, doi:10.1007/s00376-009-8211-7, 2009.

Chu, J. T., Xia, J., Xu, C. Y. and Singh, V. P.: Statistical downscaling of daily mean temperature, pan evaporation and precipitation for climate change scenarios in Haihe River, China, Theor. Appl. Climatol., 99(1–2), 149–161, doi:10.1007/s00704-009-0129-6, 2010.

Dai, A.: Increasing drought under global warming in observations and models, Nat. Clim. Chang., 3(1), 52–58, doi:10.1038/nclimate1633, 2013.

DHI (Danish Hydraulic Institute): MIKE SHE, User Manual, Volume 1: User Guide. Hørsholm: Danish Hydraulic Institute, 2014.

Dyderski, M. K., Paź, S., Frelich, L. E. and Jagodziński, A. M.: How much does climate change threaten European forest tree species distributions?, Glob. Chang. Biol., doi:10.1111/gcb.13925, 2017.

Engman, E. T.: Remote sensing in hydrology, Geophys. Monogr. Ser., 108, 165–177, doi:10.1029/GM108p0165, 1998.

Enke, W., Schneider, F. and Deutschländer, T.: A novel scheme to derive optimized circulation pattern classifications for downscaling and forecast purposes, Theor. Appl. Climatol., 82(1–2), 51–63, doi:10.1007/s00704-004-0116-x, 2005.

Feng, L., Hu, C., Chen, X., Cai, X., Tian, L. and Gan, W.: Assessment of inundation changes of Poyang Lake using MODIS observations between 2000 and 2010, Remote Sens. Environ., 121, 80–92, doi:10.1016/j.rse.2012.01.014, 2012a.

Feng, L., Hu, C., Chen, X., Tian, L. and Chen, L.: Human induced turbidity changes in Poyang Lake between 2000 and 2010: Observations from MODIS, J. Geophys. Res. Ocean., 117(7), doi:10.1029/2011JC007864, 2012b.

Giorgi, F.: Simulation of Regional Climate Using a Limited Area Model Nested in a General Circulation Model, J. Clim., 3(9), 941–963, doi:10.1175/1520-0442(1990)003<0941:SORCUA>2.0.CO;2, 1990.

Giorgi, F.: Simulation of Regional Climate Using a Limited Area Model Nested in a General Circulation Model, J. Clim., 3(9), 941–963, doi:10.1175/1520-0442(1990)003<0941:SORCUA>2.0.CO;2, 1990.

Grotch, S. L. and MacCracken, M. C.: The Use of General Circulation Models to Predict Regional Climatic Change, J. Clim., 4(3), 286–303, doi:10.1175/1520-0442(1991)004<0286:TUOGCM>2.0.CO;2, 1991.

Guo, J.L., Guo, S., Guo, J., Chen, H.: Prediction of Precipitation Change in Poyang Lake Basin. Journal of Yangtze River Scientific Research Institute, 8, 007, 2010.

Han, X., Chen, X. and Feng, L.: Four decades of winter wetland changes in Poyang Lake based on Landsat observations between 1973 and 2013, Remote Sens. Environ., 156, 426–437, doi:10.1016/j.rse.2014.10.003, 2014.

Hong X, Guo S, Guo J, et al. Projected changes of extreme precipitation characteristics in the Poyang Lake Basin based on statistical downscaling model. Journal of Water Resources Research, 3(6), 511-521, doi:10.12677/JWRR.2014.36063, 2014.

Lenderink, G., Buishand, A. and Van Deursen, W.: Estimates of future discharges of the river Rhine using two scenario methodologies: Direct versus delta approach, Hydrol. Earth Syst. Sci., 11(3), 1145–1159, doi:10.5194/hess-11-1145-2007, 2007.

Li, H., Sheffield, J. and Wood, E.: Bias correction of monthly precipitation and temperature fields from Intergovernmental Panel on Climate Change AR4 models using equidistant quantile, J. Geophys. Res., 115(10), D10101, doi:10.1029/2009JD012882, 2010.

Li, Y. L., Tao, H., Yao, J. and Zhang, Q.: Application of a distributed catchment model to investigate hydrological impacts of climate change within Poyang Lake catchment (China), Hydrol. Res., 47(S1), 120–135, doi:10.2166/nh.2016.234, 2016.

Liu, C. M., Liu, W. Bin, Fu, G. Bin and Ouyang, R. L.: A discussion of some aspects of statistical downscaling in climate impacts assessment, Shuikexue Jinzhan/Advances Water Sci., 23(3), 427–437, doi:CNKI: 32.1309.P.20120501.1616.002, 2012.

Lohmann, D., Rashke, E., Nijssen, B. and Lettenmaier, D. P.: Regional scale hydrology: I. Formulation of the VIC-2L model coupled to a routing model, Hydrol. Sci. J., 43(1), 131–141, doi:10.1080/02626669809492107, 1998.

Min, Q., Min, D.: Drought Change Characteristics and Drought Protection Countermeasures for Poyanghu Lake Basin, Journal of China Hydrology, 1, 84-88, 2010.

Min, S. K., Zhang, X., Zwiers, F. W. and Hegerl, G. C.: Human contribution to more-intense precipitation extremes, Nature, 470(7334), 378–381, doi:10.1038/nature09763, 2011.

Mullan, D., Chen, J. and Zhang, X. J.: Validation of non-stationary precipitation series for site-specific impact assessment: comparison of two statistical downscaling techniques, Clim. Dyn., 46(3–4), 967–986, doi:10.1007/s00382-015-2626-x, 2016.

Pall, P., Aina, T., Stone, D. A., Stott, P. A., Nozawa, T., Hilberts, A. G. J., Lohmann, D. and Allen, M. R.: Anthropogenic greenhouse gas contribution to flood risk in England and Wales in autumn 2000, Nature, 470(7334), 382–385, doi:10.1038/nature09762, 2011.

Prudhomme, C., Reynard, N. and Crooks, S.: Downscaling of global climate models for flood frequency analysis: Where are we now, Hydrol. Process., 16, 1137–1150, 2002.

Putnam, A. E. and Broecker, W. S.: Human-induced changes in the distribution of rainfall, Sci. Adv., 3(5), doi:10.1126/sciadv.1600871, 2017.

Riahi, K., Rao, S., Krey, V., Cho, C., Chirkov, V., Fischer, G., Kindermann, G., Nakicenovic, N. and Rafaj, P.: RCP 8.5-A scenario of comparatively high greenhouse gas emissions, Clim. Change, 109(1), 33–57, doi:10.1007/s10584-011-0149-y, 2011.

Segu, P. Q.: Comparison of three downscaling methods in simulating the impact of climate change on the hydrology of Mediterranean basins, J. Hydrol., 383, 111–124, 2010.

Sibson, R: A brief description of natural neighbour interpolation. Interpreting multivariate data, 1981.

Sperber, K. R., Annamalai, H., Kang, I. S., Kitoh, A., Moise, A., Turner, A., Wang, B. and Zhou, T.: The Asian summer monsoon: An intercomparison of CMIP5 vs. CMIP3 simulations of the late 20th century, Clim. Dyn., 41(9–10), 2711–2744, doi:10.1007/s00382-012-1607-6, 2013.

Tan, Ruizhi: A Study on the Regional Energetics during Break, Transitional and Active Periods of the Southwest Monsoon in South East Asia, SCIENTIA ATMOSPHERICA SINICA, 1994.

Taylor, K. E., Stouffer, R. J. and Meehl, G. A.: An overview of CMIP5 and the experiment desing. American Meteorological Society, Bulletim Am. Meteorol. Soc., 93, 485–498, doi:10.1175/BAMS-D-11-00094.1, 2012.

Teutschbein, C. and Seibert, J.: Bias correction of regional climate model simulations for hydrological climate-change impact studies: Review and evaluation of different methods, J. Hydrol., 456–457, 12–29, doi:10.1016/j.jhydrol.2012.05.052, 2012.

Teutschbein, C. and Seibert, J.: Is bias correction of regional climate model (RCM) simulations possible for non-stationary conditions, Hydrol. Earth Syst. Sci., 17(12), 5061–5077, doi:10.5194/hess-17-5061-2013, 2013.

Toggweiler, J. and Key, R.: Ocean circulation: Thermohaline circulation, Encycl. Atmos. Sci., 4, 1549–1555., doi:10.1002/joc, 2001.

Trenberth K E.: Changes in precipitation with climate change, Clim. Res., 47(1–2), 123–138, 2011.

Wang H, Zhao G, Peng J, et al.: Precipitation characteristics over five major river systems of Poyang drainage areas in recent 50 years. Resources and Environment in the Yangtze Basin, 7, 615-619, 2009.

Wang, J., Hong, Y., Li, L., Gourley, J. J., Khan, S. I., Yilmaz, K. K., Adler, R. F., Policelli, F. S., Habib, S., Irwn, D., Limaye, A. S., Korme, T. and Okello, L.: The coupled routing and excess storage (CREST) distributed hydrological model, Hydrol. Sci. J., 56(1), 84–98, doi:10.1080/02626667.2010.543087, 2011.

Weisheimer, R. M. A. L. A. and Guti ́errez, J. M.: Can bias correction and statistical downscaling methods improve the skill of seasonal precipitation forecasts ?, Clim. Dyn., 50(3), 1161–1176, doi:10.1007/s00382-017-3668-z, 2018.

Wilby, R. and Dawson, C. W.: SDSM 4.2-A decision support tool for the assessment of regional climate change impacts, 94, 2007.

Wilks, D. S.: Use of stochastic weather generators for precipitation downscaling, Wiley Interdiscip. Rev. Clim. Chang., 1(6), 898–907, doi:10.1002/wcc.85, 2010.

WU, G., LIU, Y., ZHAO, X., & YE, C.: Spatio-temporal variations of evapotranspiration in Poyang Lake Basin using MOD16 products, Geographical Research, 32(4), 617-627, 2013.

Wu, J., Zha, J. and Zhao, D.: Evaluating the effects of land use and cover change on the decrease of surface wind speed over China in recent 30 years using a statistical downscaling method, Clim. Dyn., 48(1–2), 131–149, doi:10.1007/s00382-016-3065-z, 2017.

Wu, Q., Nie, Q., Zhou, R.: Analysis of wind energy resources reserves and characteristics in mountain area of Jiangxi province, Journal of Natural Resources, 28(9), 1605-1614, doi: 10.11849/zrzyxb.2013.09.015, 2013.

Xu, C. Y.: From GCMs to river flow: A review of downscaling methods and hydrologic modelling approaches, Prog. Phys. Geogr., 23(2), 229–249, doi:10.1191/030913399667424608, 1999.

Ye, X., Zhang, Q., Bai, L. and Hu, Q.: A modeling study of catchment discharge to Poyang Lake under future climate in China, Quat. Int., 244(2), 221–229, doi:10.1016/j.quaint.2010.07.004, 2011.

Yuan, W.: Diurnal cycles of precipitation over subtropical China in IPCC AR5 AMIP simulations, Adv. Atmos. Sci., 30(6), 1679–1694, doi:10.1007/s00376-013-2250-9, 2013.

Yukimoto, S., Adachi, Y., Hosaka, M., et al.: A New Global Climate Model of the Meteorological Research Institute: MRI-CGCM3-Model Description and Basic Performance, J. Meteorol. Soc. Japan, 90A, 23–64, doi:10.2151/jmsj.2012-A02, 2012.

Zhan, M., Yin, J. and Zhang, Y.: Analysis on characteristic of precipitation in Poyang Lake Basin from 1959 to 2008, Procedia Environ. Sci., 10, 1526–1533, doi:10.1016/j.proenv.2011.09.243, 2011.

Zhang, L., Lu, J., Chen, X., Liang, D., Fu, X., Sauvage, S. and Perez, J. M. S.: Stream flow simulation and verification in ungauged zones by coupling hydrological and hydrodynamic models: A case study of the Poyang Lake ungauged zone, Hydrol. Earth Syst. Sci., 21(11), 5847–5861, doi:10.5194/hess-21-5847-2017, 2017.

Zhang, Q., Ye, X. chun, Werner, A. D., Li, Y. liang, Yao, J., Li, X. hu and Xu, C. yu: An investigation of enhanced recessions in Poyang Lake: Comparison of Yangtze River and local catchment impacts, J. Hydrol., 517, 425–434, doi:10.1016/j.jhydrol.2014.05.051, 2014.

Zhang, X., Wan, H., Zwiers, F. W., Hegerl, G. C. and Min, S. K.: Attributing intensification of precipitation extremes to human influence, Geophys. Res. Lett., 40(19), 5252–5257, doi:10.1002/grl.51010, 2013.

Zhao, Y., Zhu, J. and Xu, Y.: Establishment and assessment of the grid precipitation datasets in China for recent 50 years, J. Meteorol. Sci., 34(4), 4–10, 2014.

Zorita, E. and Von Storch, H.: The analog method as a simple statistical downscaling technique: Comparison with more complicated methods, J. Clim., 12, 2474–2489, doi:10.1175/1520-0442(1999)012<2474:TAMAAS>2.0.CO;2, 1999.

574 **Figures**

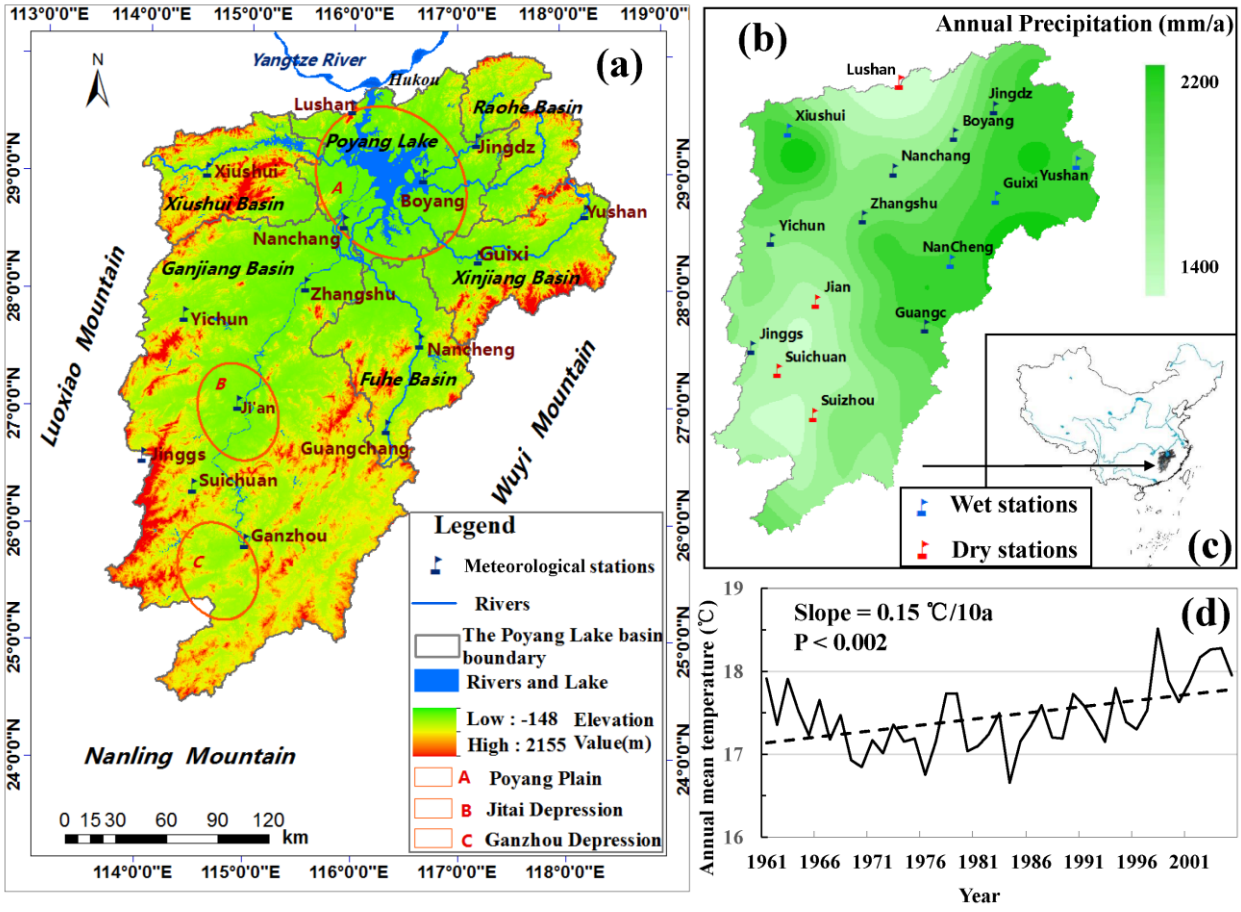

575

576 Fig. 1. The topography and landforms (a), precipitation distribution and dry-wet stations (b), temperature change (d) and
577 location of the Poyang Lake Basin (c). We sorted the annually accumulated precipitation of the 15 stations, averaged over time
578 from 1961 to 2005. The 4 stations with the max or min mean annual precipitations are set as dry or wet stations, respectively.

579

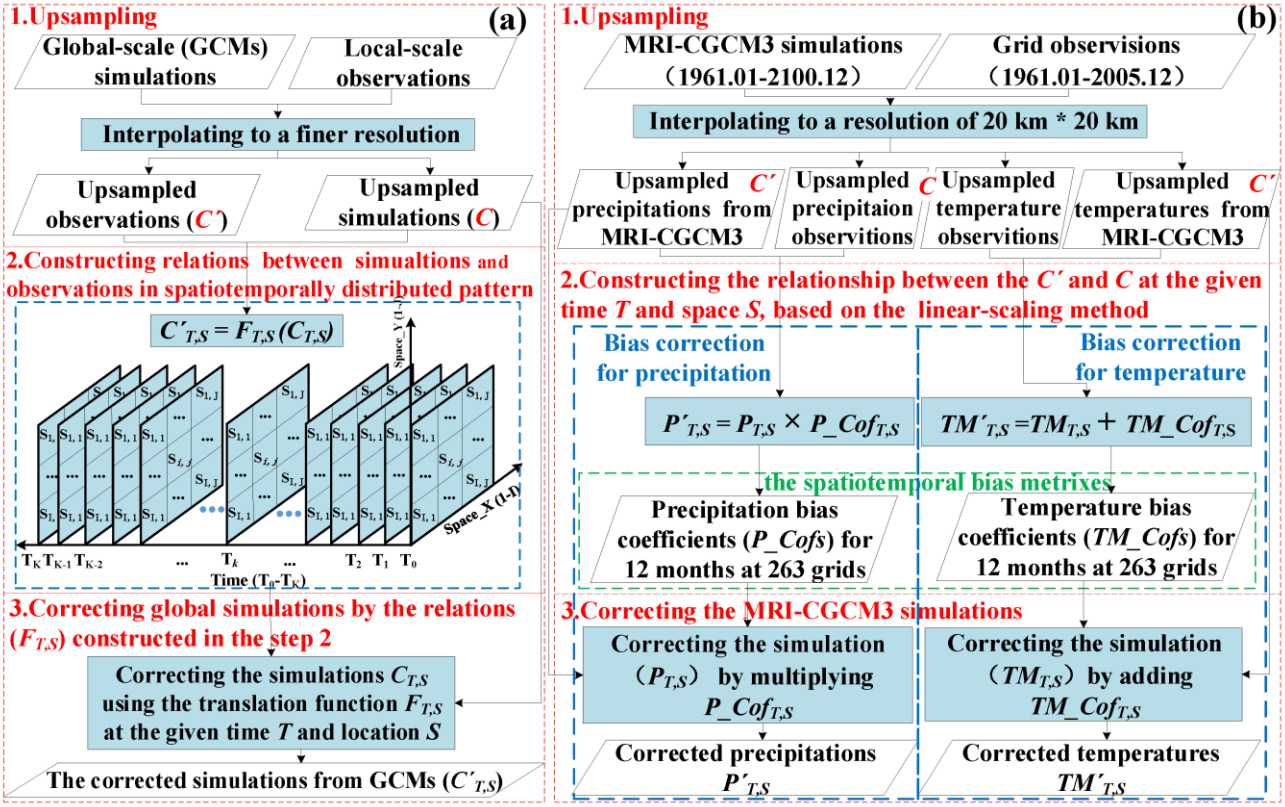

Fig. 2 Conceptual flow chart of the climate projection including upsampling, relation construction and correction: The common framework of the STDDM (a) and test case base on the linear-scaling algorithm (b). The STDDM was used to project MRI-CGCM3 simulations from 1998 to 2100.

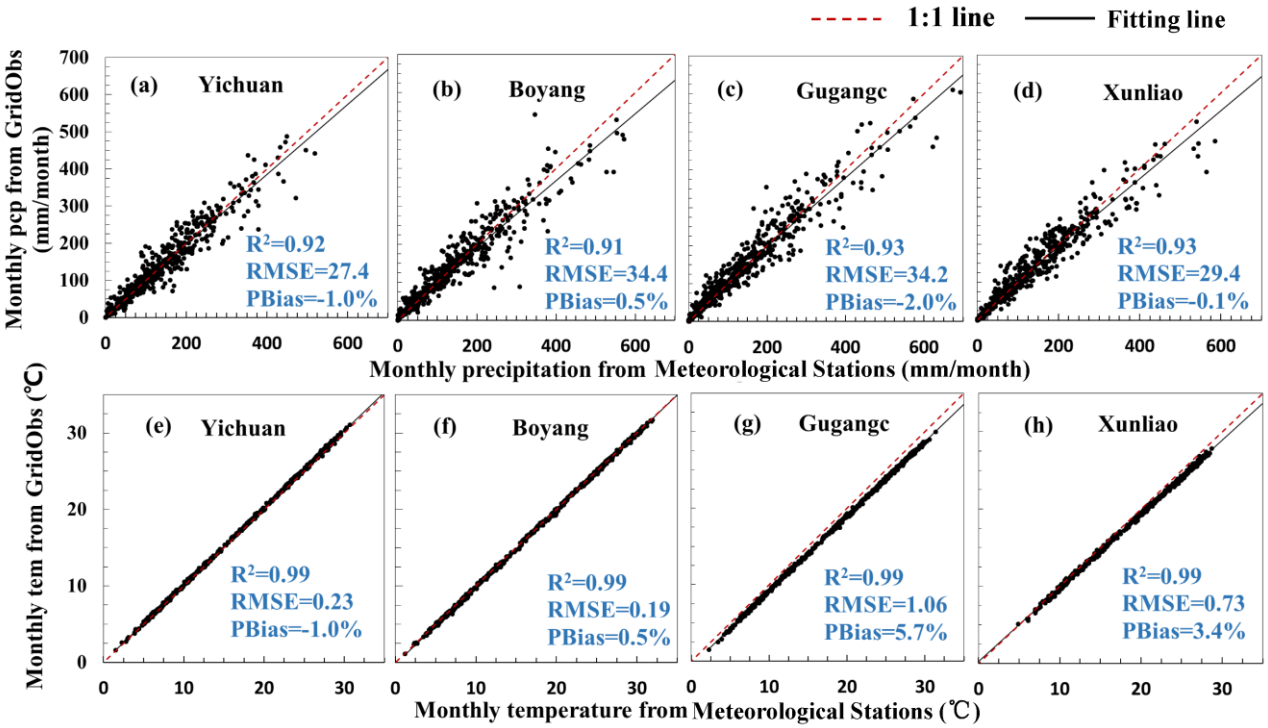

586

587 Fig. 3. Validation of gridded meteorological data (GridObs) by using gauging stations observation: Precipitation (pcp; a,b,c
588 and d) and temperature (tem; e,d,f and g) at meteorological station of Jian (a and e), Ganzhou (b and d), Zhangshu (c and f)
589 and Lushan (d and g).

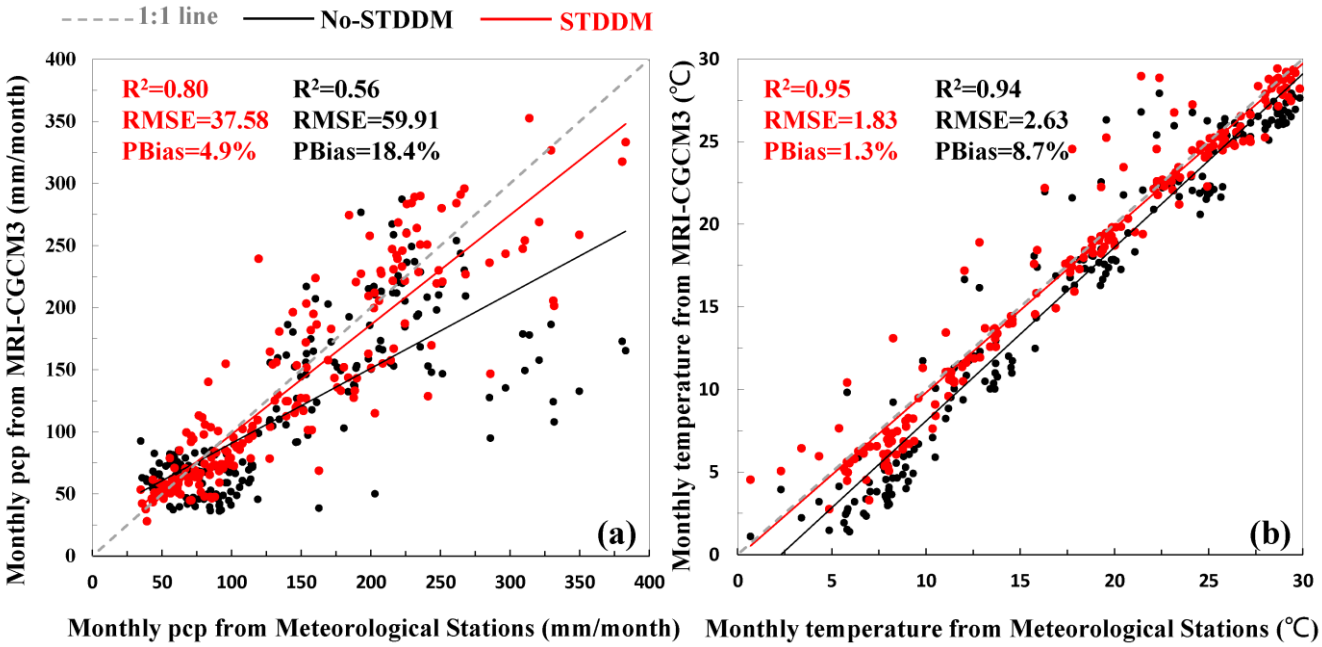

590

591 Fig. 4. Validation of the precipitation (pcp) (a) and temperature (b) projections by the STDDM (in black) and No-STDDM (in
592 red). Dots represent the monthly precipitations (or temperatures), averaged over 20 years from 1986 to 2005. The dots contain
593 monthly precipitations of the 15 stations. The solid lines represent linear regression which is the best fit through all match-ups
594 of the projections and observations.

595

596

597

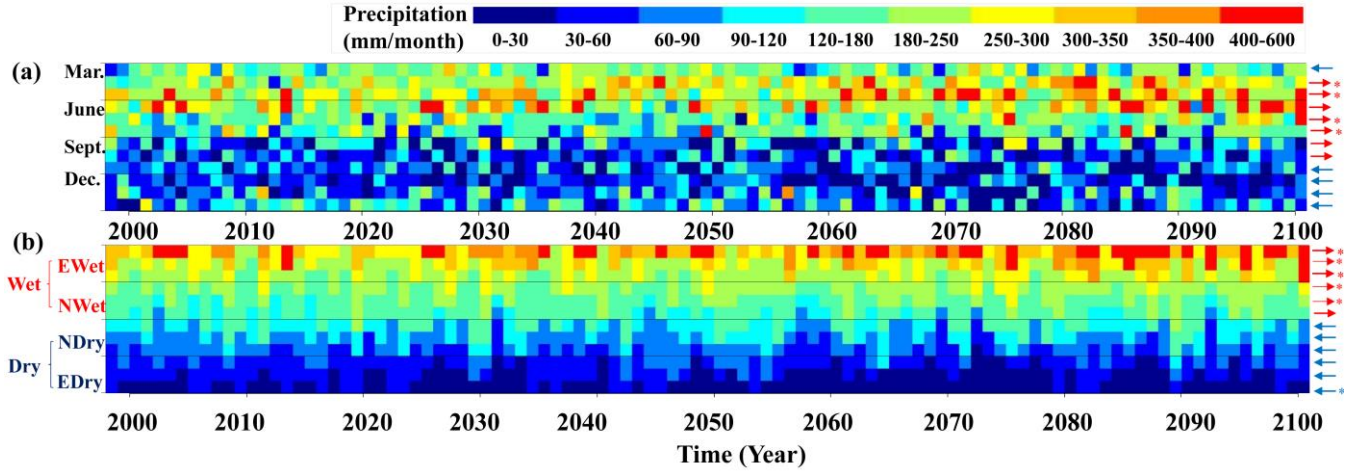

Fig. 5. Total variability of monthly precipitation from 1998 to 2100. Each column represents the data for one year and each cell represents an accumulative precipitation of one month. The red (blue) arrows indicate that the monthly precipitation experienced an increasing (decreasing) trend over the 103 years, respectively. The asterisk demonstrates the significant trends with $p<0.05$. (a) Monthly precipitation in month order, referred to Spring (March to May), summer (June to August), autumn (September to November), and winter (December to next February) from top to bottom, respectively. (b) Monthly precipitation, sorted in the descending order for each year, where months are classified as extreme wet (EWet), normal wet (NWet), normal dry (NDry) and extreme dry (Edry) months from up to down. Therein, wet months (Wet) include extreme and normal wet ones while dry months (Dry) include extreme and normal dry ones.

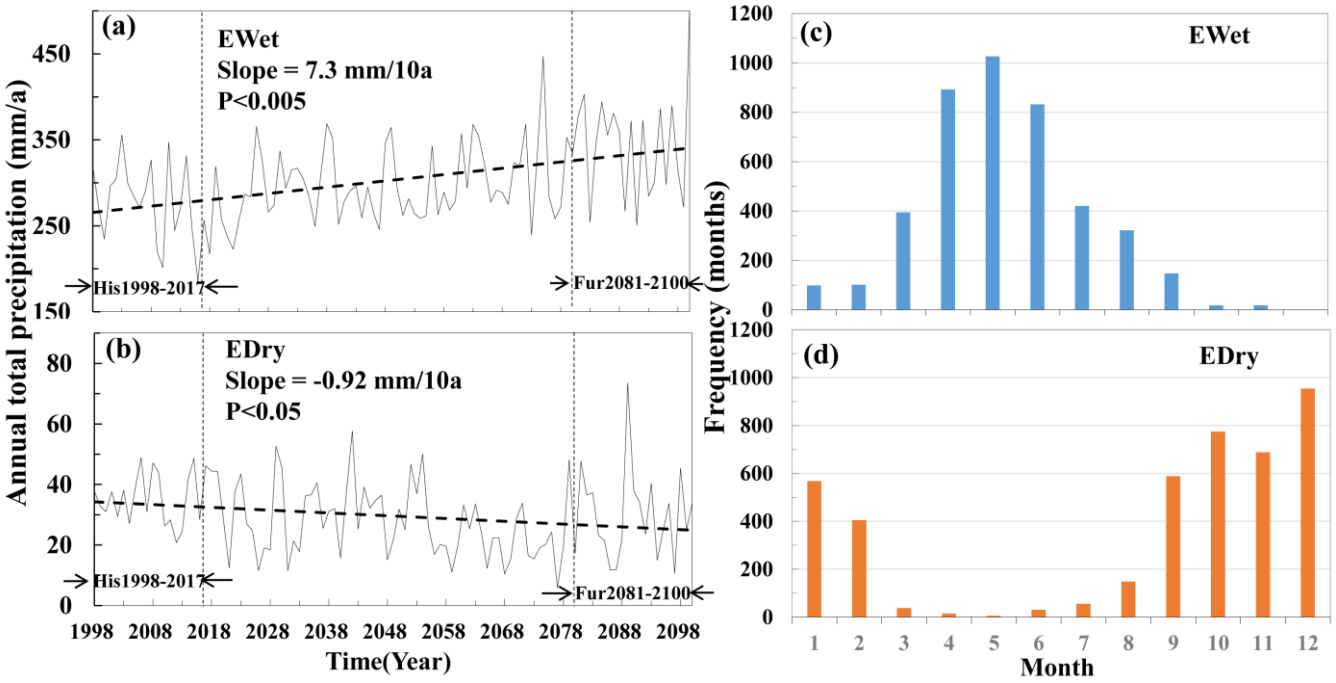

Fig. 6. The trends of changes in monthly precipitations of extreme wet (EWet) (a) and dry (EDry) (b) months from 1998 to 2100. The further future period from 2081 to 2100 (Fur2081-2100) and baseline period from 1998 to 2017 (His1998-2017) are indicated by arrows. Frequencies of the months in extreme wet (c) or dry (d) months are calculated during the period from 1998 to 2100.

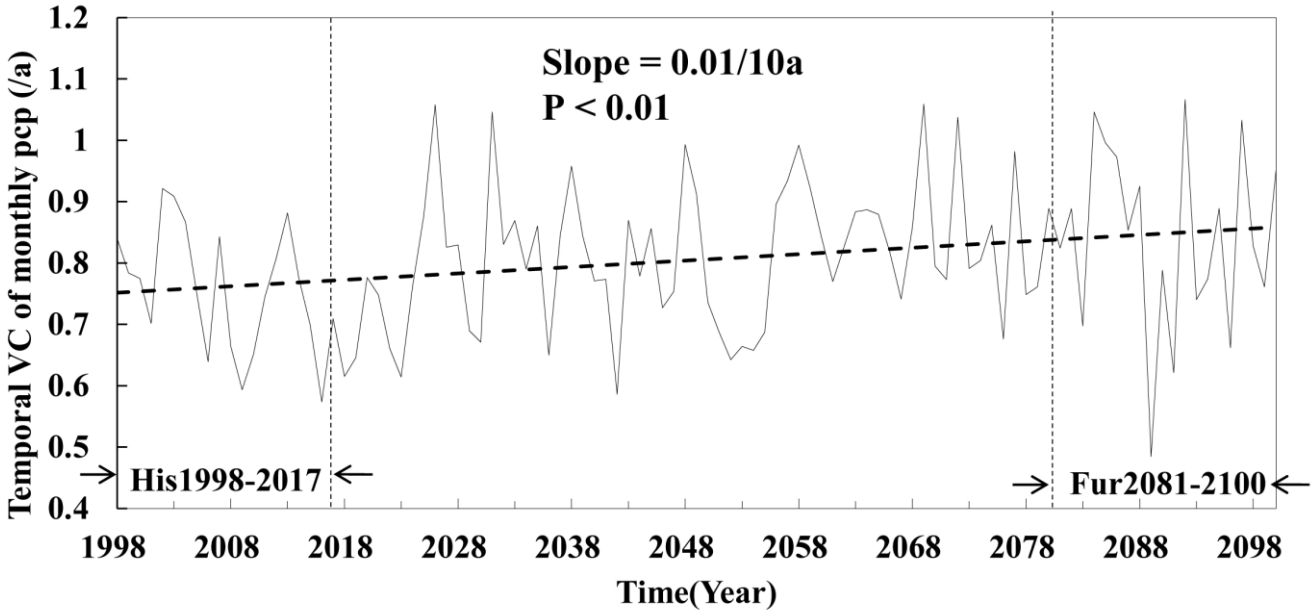

614

615 Fig. 7. The temporal variation coefficients of the extreme month precipitations for each year over 1988 to 2100. The extreme
616 months are composed of the extreme wet and dry months. The far future period from 2081 to 2100 (Fur2081-2100) and baseline
617 period from 1998 to 2017 (His1998-2017) are indicated by arrows.

618

619

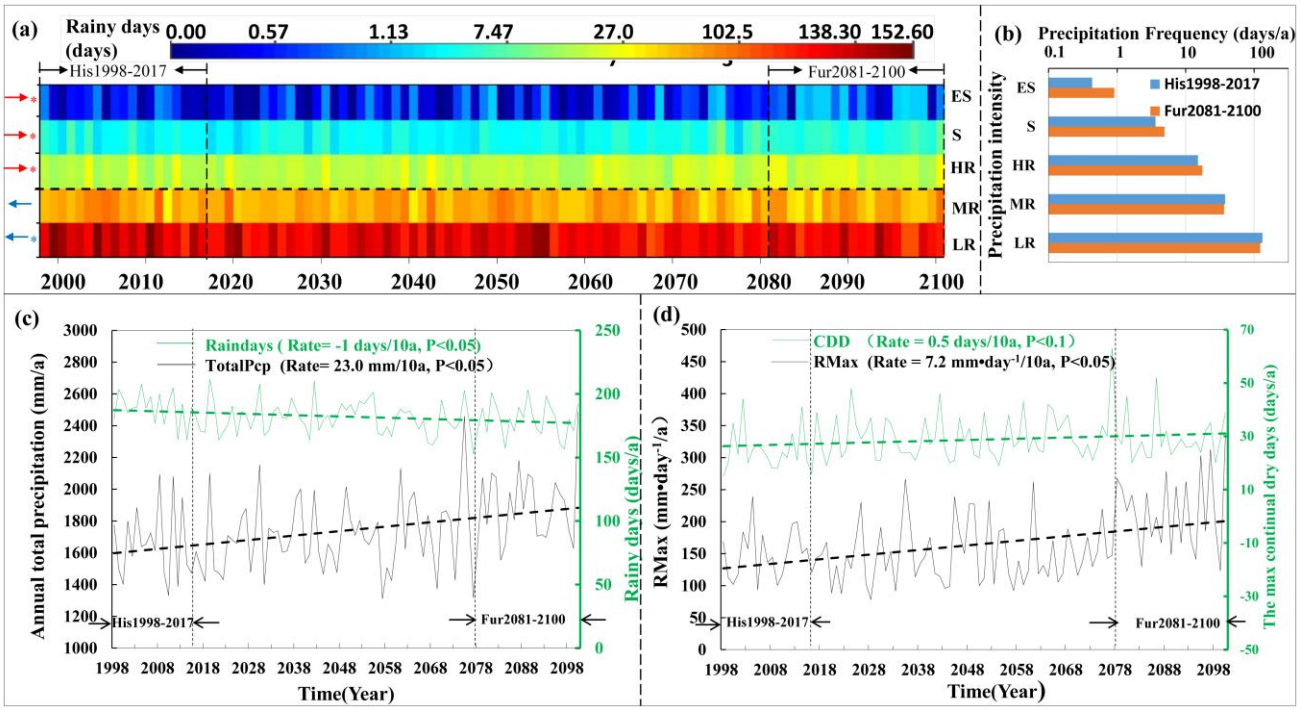

Fig. 8. The changes in daily precipitation intensities and frequencies. (a) Precipitation intensities and frequencies for each year over 1998 to 2100, where each column represents a year and each row indicates a precipitation intensity. Daily precipitation intensities are categorized to 5 classes, Light Rain (LR), Median Rain (MR), Heavy Rain (HR), Rainstorm (S), and Extreme Rainstorm (ES) with daily precipitation of 0.1-10, 10-25, 25-50, 50-100 and >100 mm/day, respectively. The moderate rain includes LR and MR while the extreme rain is composed of HR, S, and ES. The cell represents an annual frequency of one precipitation intensity, with a unit of days. The red (blue) arrows indicate that annual frequency of the precipitation intensity experienced an increasing (decreasing) trends over the 103 years (from 1998 to 2100), respectively. The asterisk represents the significant trends with $p<0.05$. The far future period from 2081 to 2100 (Fur2081-2100) and baseline period from 1998 to 2017 (His1998-2017) are indicated by arrows. (b) Precipitation frequencies of LR, MR, HR, S, and ES for Fur2081-2100 and His1998-2017, respectively. (c) The change of the long-term data for annual total precipitation (totalPcp) and total rainy days (Raindays). (d) The change of the long-term data for annual max daily precipitation (RMax) and annual max continuous dry days (CCD).

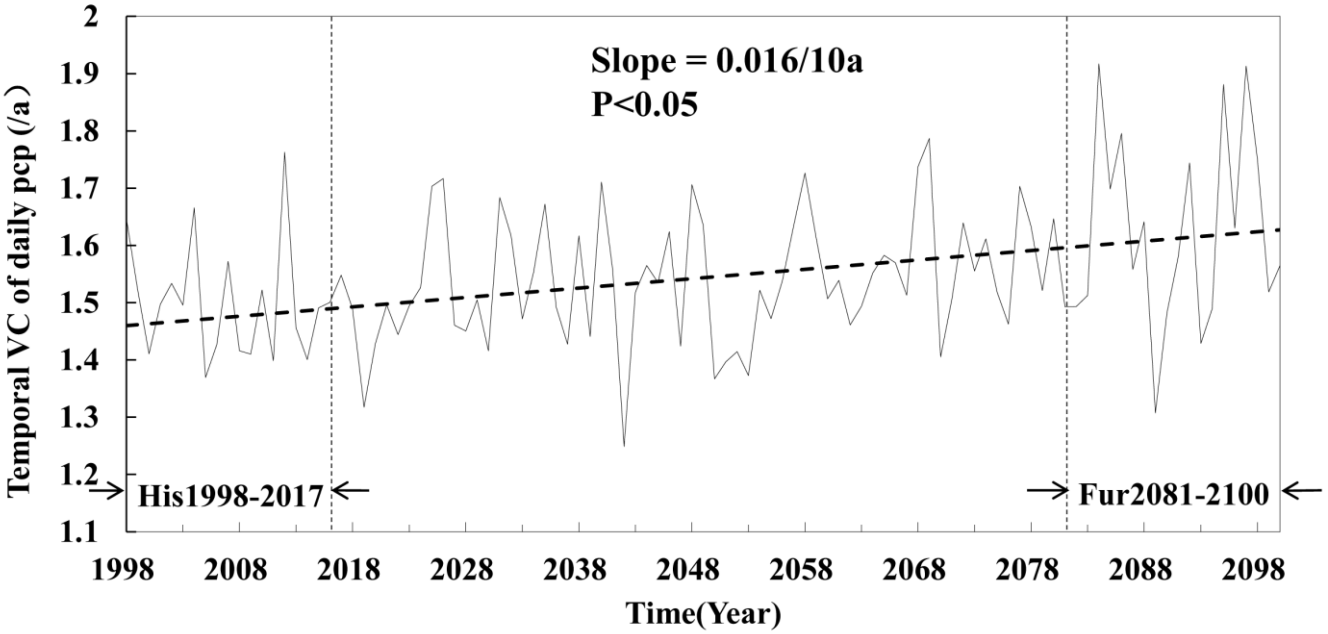

634

635 Fig. 9. The temporal variation coefficient of daily precipitations for each year over 1988 to 2100. The far future period from

636 2081 to 2100 (Fur2081-2100) and baseline period from 1998 to 2017 (His1998-2017) are indicated by arrows.

637

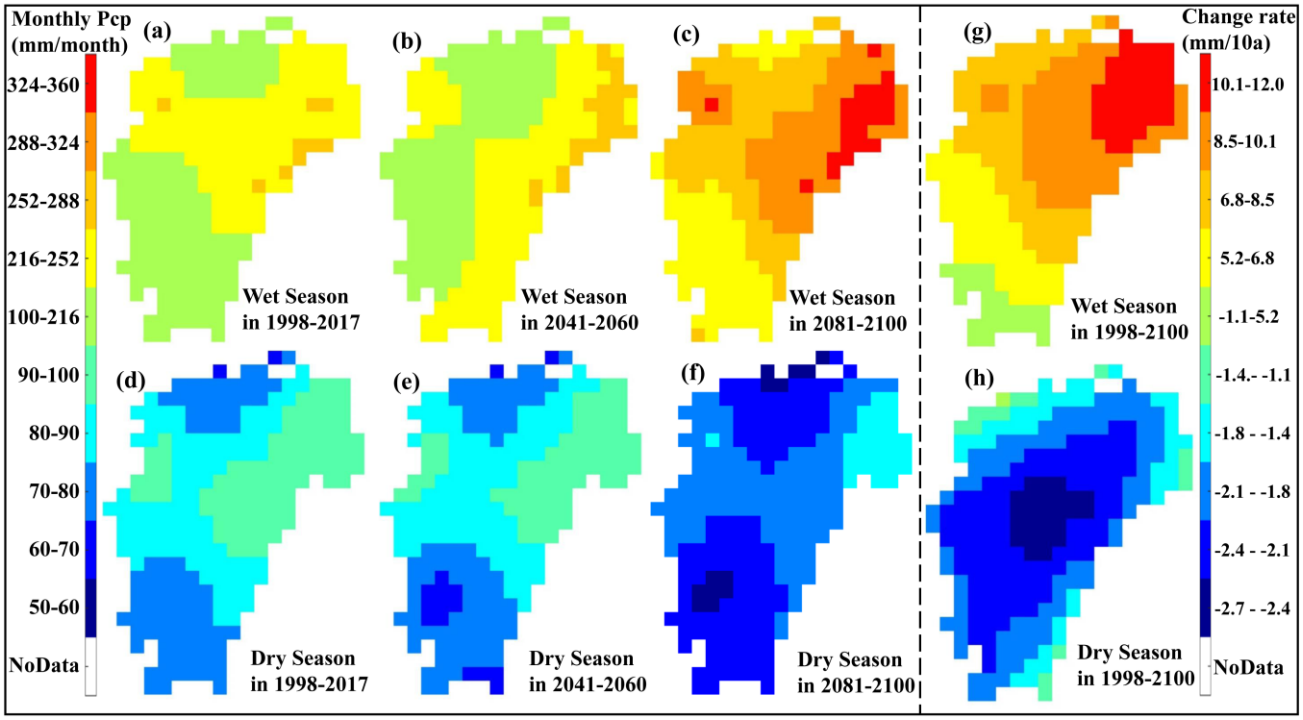

Fig. 10. The precipitation changes in the spatial pattern during the period from 1998 to 2100: average monthly precipitations of the wet season (April to July) during the period from 1998 to 2017 (a), 2041 to 2060 (b), and 2081 to 2100 (c); average monthly precipitations of the dry season (December to next February) during the historical period from 1998 to 2017 (d), 2041 to 2060 (e), and 2081 to 2100 (f); change rate of monthly precipitation in wet (g) and dry (h) season from 1998 to 2100. As floods and droughts occur more frequently in extreme months, the precipitation in the analysis considered only the extreme wet (April-July) and dry (September-February) months (Fig. 5c and d). Besides, precipitation is dominated by southeast summer monsoon, which brings water vapor from the sea. The summer monsoon is frequent from the end of spring and stat of autumn, covering the wet months April to July. However, though as dry months, the autumn period from September to November is affected by southeast summer monsoon (Tan et al., 1994) slightly because autumns are the transpiration periods of summer to winter. Therefore, winter (December-February) was represented as the dry season with poor rain; while April-July was represented as the wet season with abundant rain.

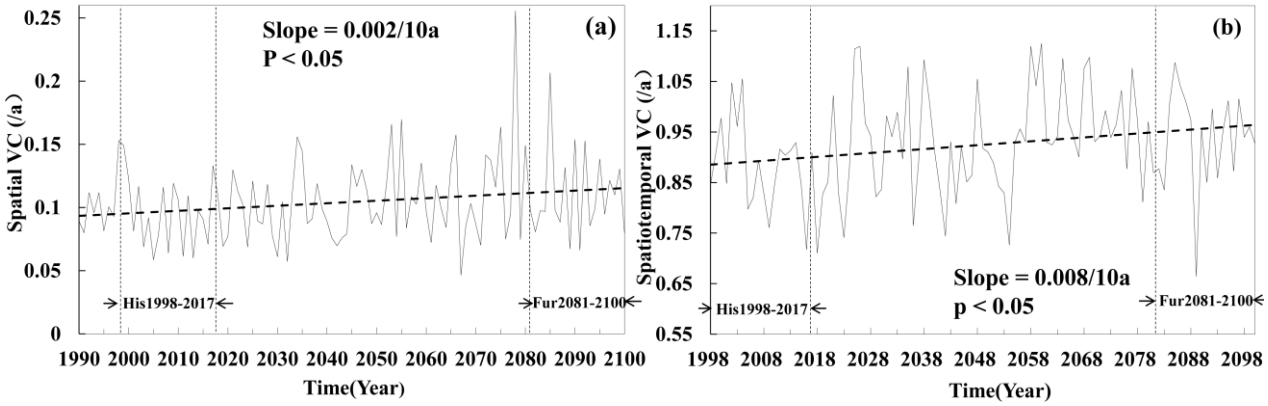

Fig. 11. The spatial (a) and spatiotemporal (b) variation coefficient for each year over 1988 to 2100. The further future period from 2081 to 2100 (Fur2081-2100) and baseline period from 1998 to 2017 (His1998-2017) are indicated by arrows.

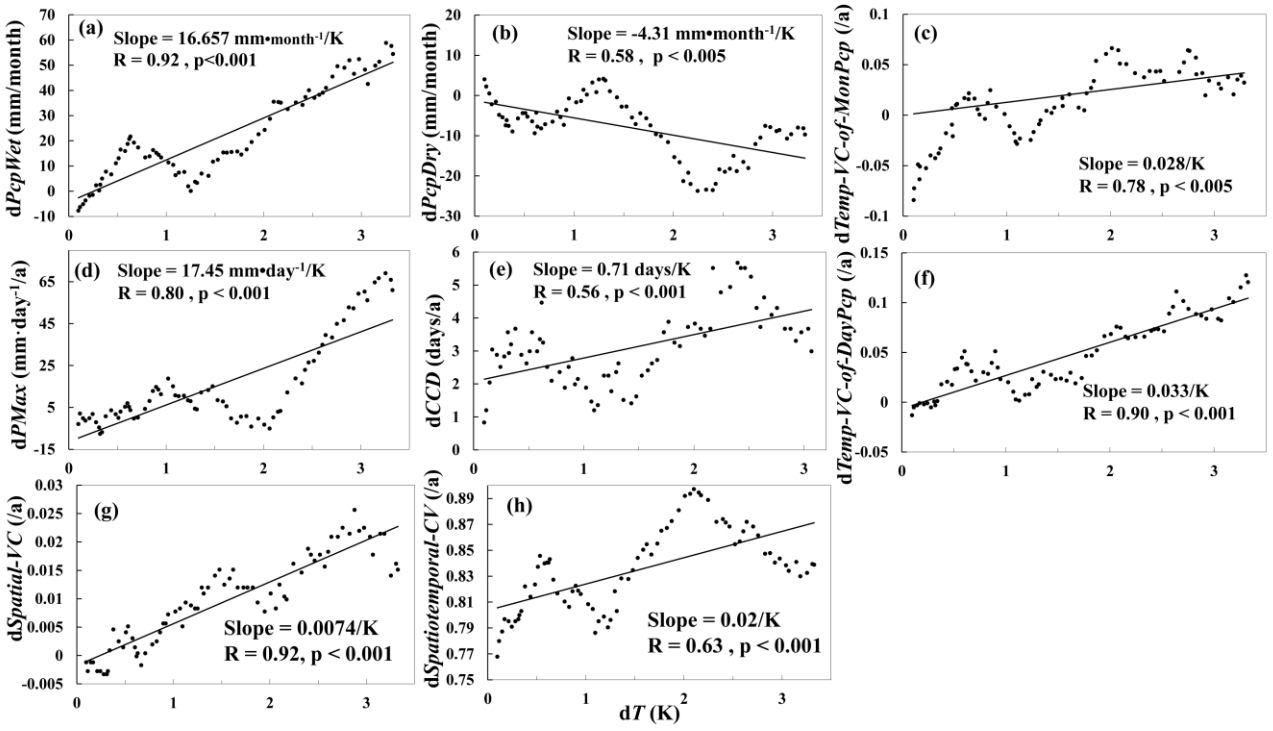

Fig. 12. The relationship between the precipitation index changes (d*PcpIndex*) and the temperature increment (d*T*). The precipitation indexes include annual precipitation in the wet season (PcpWet) (a), annual precipitation in the dry season (PcpDry) (b), temporal variance coefficient of monthly precipitations (Temp-VC-of-MonPcp) (c), annual max daily precipitation (PMax) (d), annual max continuous dry days (CCD) (e), temporal variance coefficient of daily precipitations (Temp-VC-of-DayPcp) (f), spatial variance coefficient (Spatial-VC) (g), and spatiotemporal variance coefficient (Spatiotemporal-VC) (h). All the precipitation index changes show significant correlations with temperature increment.